Molecular Neurobiology (2019) 56:954–962
https://doi.org/10.1007/s12035-018-1137-2

Multimodal Molecular Imaging Demonstrates Myeloperoxidase Regulation of Matrix Metalloproteinase Activity in Neuroinflammation

Yinian Zhang[1,2] · Huateng Dong[2,3] · Daniel P. Seeburg[2,4] · Gregory R. Wojtkiewicz[2] · Peter Waterman[2] · Benjamin Pulli[2] · Reza Forghani[2,5] · Muhammad Ali[2] · Yoshiko Iwamoto[2] · Filip K. Swirski[2] · John W. Chen[2]

Received: 8 September 2017 / Accepted: 18 May 2018 / Published online: 28 May 2018

Abstract

Myeloperoxidase (MPO) has paradoxically been found to be able to both activate matrix metalloproteinases (MMPs) as well as inhibit MMPs. However, these regulatory effects have not yet been observed in vivo, and it is unclear which pathway is relevant in vivo. We aim to track MPO regulation of MMP activity in living animals in neuroinflammation. Mice induced with experimental autoimmune encephalomyelitis (EAE), a mouse model of neuroinflammation and multiple sclerosis, were treated with either the MPO-specific inhibitor 4-aminobenzoic acid hydrazide or saline as control. Mice underwent concurrent magnetic resonance imaging (MRI) with the MPO-specific molecular imaging agent MPO-Gd and fluorescence molecular tomography (FMT) with the MMP-targeting agent MMPsense on day 12 after induction. Biochemical and histopathological correlations were performed. Utilizing concurrent MRI and FMT imaging, we found reduced MMP activity in the brain with MPO inhibition, demonstrating MPO activity positively regulates MMP activity in vivo. In vivo MMPSense activation and MMP-9 activity correlated with MPO-Gd$^+$ lesion volume and disease severity. This was corroborated by in vitro assays and histopathological analyses that showed MMP activity and MMP-9$^+$ cells correlated with MPO activity and MPO$^+$ cells. In conclusion, multimodal molecular imaging demonstrates for the first time MPO regulation of MMP activity in living animals. This approach could serve as a model to study the interactions of other biologically interesting molecules in living organisms.

Keywords Myeloperoxidase · Matrix metalloproteinases · Neuroinflammation · Experimental autoimmune encephalomyelitis · Fluorescence molecular tomography · Magnetic resonance imaging

Yinian Zhang and Huateng Dong contributed equally to this work.

Electronic supplementary material The online version of this article (https://doi.org/10.1007/s12035-018-1137-2) contains supplementary material, which is available to authorized users.

✉ John W. Chen
jwchen@mgh.harvard.edu

[1] Department of Neurosurgery, Institute of Neurology, Lanzhou University Second Hospital, 82 Cuiying Men Road, Lanzhou 730030, China

[2] Center for Systems Biology and Institute for Innovation in Imaging, Department of Radiology, Harvard Medical School, Massachusetts General Hospital, 185 Cambridge Street, 5.210 Richard B. Simches Research Building, Boston, MA 02114, USA

[3] Present address: Department of Pediatric Neurology, Gansu Provincial Maternity and Child-Care Hospital, Lanzhou 730050, China

[4] Neuroradiology Section, Charlotte Radiology, 1701 East Blvd, Charlotte, NC 28203, USA

[5] Department of Radiology, Jewish General Hospital and McGill University, 3755 Cote Ste-Catherine Road, Montreal, QC, Canada

Introduction

Among a wide variety of proteolytic enzymes, the matrix metalloproteinase (MMP) family, comprising over 20 enzyme subtypes, has received much attention in neuroinflammatory diseases. Multiple clinical studies have shown a correlation between elevated MMP expression and poor outcome in neurological diseases [1–3]. Blood-brain barrier (BBB) disruption is usually followed by infiltration of leukocytes, which can aggravate immune reactions along with microglial activation. The entry of leukocytes into the CNS is dependent on several factors, including the expression of MMPs, which degrade the extracellular matrix (ECM) proteins of the basal lamina that surrounds blood vessels [4].

MMPs are endopeptidases characterized by a conserved Zn^{2+}-binding motif in the catalytic domain and several conserved protein domains [5]. MMP expression is transcriptionally regulated by a variety of factors, including pro-inflammatory cytokines, growth factors, and hormones. During inflammation, leukocyte traffic through tissue barriers

is only possible if these cells are equipped with proteases to remodel the extracellular matrix (ECM). MMPs are therefore crucial effector molecules of inflammatory cells [3]. In particular, MMP-9 is an important immune effector molecule in multiple sclerosis (MS) pathogenesis [4, 6] and is a key protease involved in MS, experimental autoimmune encephalomyelitis (EAE), and neuroinflammation [7]. It functions in cell migration through connective tissues and vessel walls and damages the BBB. It also lyses protein substrates, such as myelin proteins, cell-adhesion molecules, cytokines, and chemokines that are relevant in MS and other neurological diseases [6]. In murine EAE, both MMP-2 and MMP-9 are upregulated during the development of the disease syndrome [1]. However, how MMPs are regulated in vivo by endogenous factors in living organisms has not yet been studied.

One potential modulator of MMP activity is myeloperoxidase (MPO). MPO is a potent oxidative mediator found in leukocytes [8]. It is the most abundant component in azurophilic granules in neutrophils and is also expressed in other cells in the myeloid line, especially Ly-6C^{high} monocytes [9] and activated microglia/macrophages [10]. By generating oxidizing species such as hypochlorous acid (HOCl), MPO has been found in in vitro studies to be able to activate MMPs, both directly by modifying MMPs [11] and indirectly by inhibiting tissue inhibitors of metalloproteinases (TIMP) [12]. Paradoxically, MPO activity can also directly inhibit MMPs by altering the active domain [13]. These regulatory effects have not yet been observed in vivo, and it is unclear which mechanism is relevant in vivo. Therefore, in this study, we aim to track MPO regulation of MMP activity in vivo using a multimodal molecular imaging approach in experimental autoimmune encephalomyelitis (EAE), a mouse model of neuroinflammation and the clinical disease multiple sclerosis.

Materials and Methods

Experimental Autoimmune Encephalomyelitis (EAE)

The protocol for animal experiments was approved by the institutional animal care committee. On hundred ten mice were used for the experiments (Fig. S1). EAE was induced in SJL female mice (7–10 weeks old, NCI/Frederick's) with proteolipid protein ($PLP_{139–151}$, Cat#63912, AnaSpec, Fremont, CA). One milligram of PLP and 4 mg *M. tuberculosis* H37RA (231141, Diflo, Detroit, MI) were dissolved in 0.5 ml dH_2O and 0.5 ml complete Freud's adjuvant (F5881, Sigma-Aldrich, St Louis, MO). The content was emulsified by a tissue homogenizer (Cat#15–338-420, Fisher Scientific, Waltham, MA) for 3 min at 15,000 rpm. Each mouse received 100 μl of the PLP emulsion (subcutaneously, 25 μl each in the bilateral inguinal and axillary regions). On day 0 and day 2, 0.1 μg pertussingen (P7208, Sigma-Aldrich) in 0.2 ml of PBS was injected intravenously. Animals were weighed and monitored at least daily after immunization. Since daily dosing of mice with a potential therapeutic often delays the onset of EAE and decreases severity of EAE due to stress of the procedures, we performed sham injections (400 μl saline) for 4 to 7 days before EAE induction to reduce the effects of stress. When the saline-treated group reaches the first paralytic episode (~day 12) the mice were used for the experiments below.

Therapeutic Intervention

After EAE induction, mice in the treatment cohort received the specific irreversible MPO inhibitor 4-aminobenzoic hydrazide (ABAH) (40 mg/kg, A41909, Sigma-Aldrich) by intraperitoneal injection twice a day. We injected the same volume of saline (vehicle) for another group as control.

In Vivo Fluorescence Molecular Tomographic Imaging and Image Fusion

Fluorescence molecular tomography (FMT2500, PerkinElmer, Waltham MA) is a non-invasive optical imaging method that generates three-dimensional images of fluorescent signals in deep tissues. Mice received 2 nmol of MMPSense-680 (10126, PerkinElmer) via tail vein injection on day 11 after immunization (the onset of disease) and were imaged 18–24 h later. The sensor is optically silent in the unactivated state, becoming highly fluorescent when activated. The probes are based on polymeric scaffolds that can be cleaved by the target protease, resulting in the release of fluorochromes and fluorescence generation (dequenching). MMPSense-680 excitation and emission wavelength are 680 and 710 nm, respectively. Mice were anesthetized by inhalation of isoflurane 24 h after administration of the probes, and hair from head and neck was removed by shaving and chemical depilation, and rendered immobile in a multimodal imaging cartridge [14] with eight fillable fiducial markers built in, four on the bottom and four on the top. The fiducial markers are automatically added to the FMT image after reconstruction since the multimodal imaging cartridge is always in the same position in the scanner. A scan region was selected over the brain and comprised approximately 30 scan points. Imaging took approximately 5 min per mouse. Following imaging mice were transferred to MRI for co-registration imaging.

In Vivo Molecular Magnetic Resonance Imaging (MRI)

We then performed MPO-Gd (bis-5HT-DTPA-Gd) molecular MRI imaging [15, 16]. In addition to revealing the burden of MPO-positive plaques, the degree of MPO-Gd enhancement is a marker for MPO-derived oxidative stress in vivo [17]. The catalytic activation of the MPO-Gd agent oxidizes the 5-hydroxytryptamide (5HT) moiety results in agent

oligomerization and protein binding that shorten T_1 relaxivity and increase tissue retention of the activated agent [16, 17]. MR imaging was performed using a 4.7 T MRI scanner (Bruker Biosciences, Billerica, MA) with a 6- and a 2.2-cm volume coil under respiration-monitored isoflurane anesthesia. After filling the fiducials with water, the multimodal imaging cassette was placed into a custom-built holder that fits into the 6 cm volume coil and imaged with a RARE T1-weighted scan (TR = 1200 ms, TE = 14.1 ms, eight averages, RARE factor 4, 256 × 256 × 24 matrix, 0.234 × 0.234 × 1.2 mm voxels). The mouse was removed from the cassette, and a catheter was placed in the tail vein and positioned on the normal animal bed. The brain was then imaged with the 2.2 cm volume coil for higher resolution images. Pre- and post-contrast spin-echo T1-weighted images (TR = 800 s, TE = 13 s, four signal acquired, acquisition time of 6 min 57 s, matrix size 192 × 192, field of view 2.5 × 2.5 cm^2, slice thickness 0.7 mm, and 16 sections were acquired) were obtained at 0, 15, 30, 45, and 60 min after intravenous administration of 0.3 mmol/kg of MPO-Gd.

Image Fusion

For image fusion, the brain on the 6.0 cm volume coil MR images (after lanczos interpolated into the same voxel dimension as the higher resolution MR image) and the 2.2 cm volume coil images were segmented manually. A rigid affine registration using the maximum of the sum of a voxel by voxel multiplication of the two images as a similarity measure was used to register these images based on the binary images of the brain. The 6.0 cm MRI T1-weighted image was again lanczos interpolated using the affine parameters obtained from the registration. Finally, by using the multimodal fiducial markers of the imaging cassette, a simple affine registration is performed using these as control points by transforming the FMT image using lanczos interpolation. The fusion was performed in this manner to maintain the integrity of the high-resolution MPO-Gd MR images. Image processing and visualization were performed in Amira (Thermo Fisher Scientific, Waltham, MA) and MATLAB (MathWorks, Natick, MA) software.

Biochemical and Histopathologic Experiments

Please see Supplemental Methods for additional detail on the following experiments.

Flow Cytometry Excised brain specimens were evaluated for the presence of MMPs in neutrophils, monocytes, macrophages/microglia, and lymphocytes.

MPO Activity Assays Excised brain specimens were evaluated for MPO activity by using 10-acetyl-3,7-di-hydroxyphenoxazine (AAT Bioquest, Sunnyvale, CA) at an excitation wavelength of 535 nm and an emission wavelength of 590 nm.

Histopathological Analyses Fresh-frozen sections of brains were evaluated for the presence of MPO and MMP-9. For each section, we counted the total number of cells positive for either MPO or MMP-9 over the entire brain slice (60–70 high power fields). For each mouse, three different slices were analyzed and averaged.

MMP-9 Activity Assay and In Vitro Stimulation with MPO Enzyme MMP-9 activity was assayed using SensoLyte 520 MMP-9 assay kit (AnaSpec, Fremont, CA). Naïve brain extracts were stimulated in vitro by human neutrophil myeloperoxidase (10 μg/ml, Cat#426-10, Lee Solution, St Louis, MO) and then collected for the MMP-9 activity assay.

Image and Statistical Analysis

Contrast-to-noise ratios (CNRs) were computed for each region of interest (ROI, Fig. S2) according to the formula: $CNR = (ROI_{lesion} - ROI_{muscle})/SD_{noise}$, where ROI_{lesion} is the ROI of a lesion. ROI_{muscle} indicates the background, and SD_{noise} is the standard deviation of noise from an ROI measuring empty space [14]. The precontrast CNR was subtracted from the CNR at each time point to correct for any inherent T1 signal prior to contrast administration. Because early enhancement represents mostly leakage through blood-brain barrier breakdown, while delayed enhancement is derived from agent retention caused by MPO activation, we computed in vivo MPO activity (lesion activation ratio, LAR) by dividing the CNRs of lesions on delayed (60 min) over those of early (6 min) contrast-enhanced images [15, 18]. ROIs with LAR ≥ 1.8 [15] represent areas of elevated MPO activity and were included in the quantitative LAR analysis. This lesion analysis was performed over all the brain slices for each mouse by measuring the LAR of suspected areas of enhancement. For volumetric analysis, the area of the MPO+ lesions was multiplied by the slice thickness to arrive at the lesion volume. FMT data analysis was performed on three-dimensional tomographic data obtained in the 680 imaging channel. 3D data were reconstructed using a normalized Born approach. Three-dimensional volume of interest was drawn over the entire brain by referencing the MRI data [14]. Data were calculated as mean concentration in nanomolar and total amount in picomoles. Two readers (YZ and JWC, radiologists, each with more than 10 years of experience performing similar analysis) blinded to the group identities performed the analysis. The data were tested for normality using the D'Agostino-Pearson normality test and for equality of variances using the Bartlett's test. If normality and equality of variances are not rejected at the 0.05 significance level, the group means were compared using parametric analysis, such as *t* test and ANOVA. For non-

normally distributed data, nonparametric tests such as Mann-Whitney *U* test were used. A *P* value < 0.05 was considered to indicate a statistically significant difference. Correlations analyses were performed using the Pearson's correlation test. All results were reported with standard errors of measurement, except where otherwise indicated. All statistical computations were performed using Prism 5.0 (GraphPad Software, Inc., La Jolla, CA).

Results

MMP Activity in Activated Myeloid Cells in EAE Mice

We first determined the source of MMP activity in the EAE brain. At 12 days after immunization, the brain accumulated different types of leukocytes and 34% ± 5% of these cells were MMP+ (Fig. 1a). These cells constituted the primary source of MMP activity in EAE mice (Fig. 1b). Taking into account the abundance of each cell type in the brain to derive the enzyme activity of single cells (mean fluorescence intensity, MFI), microglia/monocytes/macrophages (MMM) cells had the highest MFI per cell of the myeloid cell subsets (Fig. 1b), indicating that MMM cells have the highest MMP expression. Moreover, MMM cells also dominate the overall contribution to MMP expression (Fig. 1c). Within the MMM populations, most of the MMP activity was derived from Ly-6C^{high} cells (73%), which are activated, inflammatory macrophage/microglia, but much less from Ly-6C^{low} resident microglia (27%) (Fig. 1d).

MPO and MMP-9 Activity in EAE

MPO activity correlated with disease severity ($r = 0.42$, $P = 0.014$, $n = 30$, Fig. 2a). MMP-9 activity from MMM cells also positively correlated with disease severity ($r = 0.62$, $P = 0.038$, $n = 9$, Fig. 2b). Interestingly, MPO activity and MMP-9 activity strongly correlated with each other in brain extracts of EAE mice (Fig. 2c, $r = 0.97$, $P < 0.0001$, $n = 10$). Therefore, we next sought to determine how these biomarkers interact in living animals.

Noninvasively Mapping of MPO and MMP Activity In Vivo with Concurrent MRI and FMT

As expected, molecular MPO imaging showed fewer lesions in ABAH-treated EAE mice compared to saline-treated EAE mice (Fig. 3a). Correspondingly, the mean MPO-Gd activation (LAR) decreased with MPO inhibition (Fig. 3b left panel, 5.4 ± 1.5 vs 2.2 ± 0.5, $P = 0.04$, $n = 10$ per group). There was a significant positive correlation between MPO-Gd CNR with clinical scores ($r = 0.63$, $P = 0.01$, $n = 7$, Fig. 3c, upper panel). Similarly, mean MMP activity quantified from FMT images

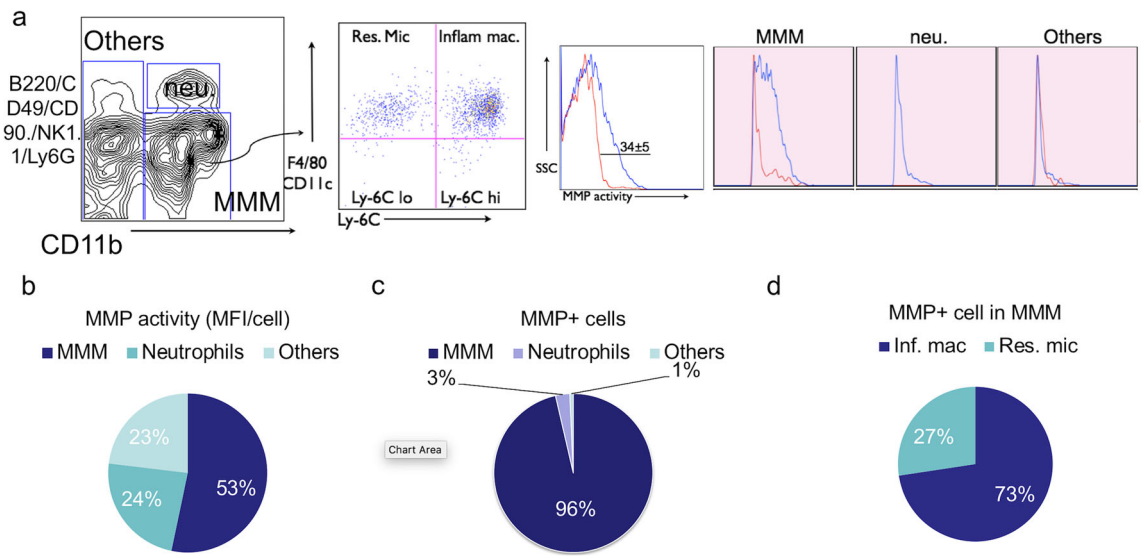

Fig. 1 Myeloid cells are the main source of matrix metalloproteinase (MMP) activity in EAE. **a** Cell surface markers used to subdivide cells into various subsets of leukocytes in the brain of saline-treated control EAE mice 12 days after immunization. Numbers denote percent MMP-positive cells in the saline (34% ± 5%) group (red line: percent MMP-positive cells in sham mice; blue line: percent MMP-positive cells in EAE mice). **b** Flow cytometric analysis revealed MMP activity mainly derived from microglia/monocytes/macrophages (MMM) in brains of EAE mice (53%). **c** MMP mean fluorescence intensity (MFI) per cell for different cell types in brain, as identified by flow cytometry. MMM cells contribute to most of the MMP activity (96%). **d** The percentage of MMP-positive cells in inflammatory macrophages and resident microglia, 73 and 27% respectively. SSC side scatter, neu. neutrophils, MMM microglia/monocytes/macrophages, MFI mean fluorescence intensity, Inf. mac inflammatory macrophages, Res. Mic resident microglia

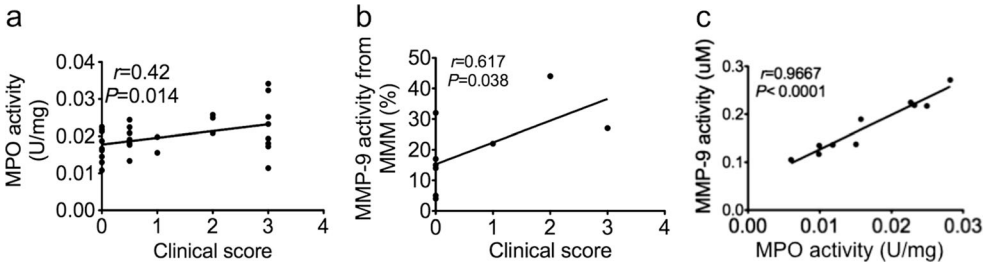

Fig. 2 MPO and MMP-9 activities correlate with disease severity, and that the two are strongly correlated. **a** Peroxidase activity correlated with clinical score ($n = 30$). **b** MMP activity from microglia/monocytes/macrophages in vitro correlated with clinical score ($n = 8$). **c** MMP-9 activity positively correlated to peroxidase activity ($n = 10$, data were obtained by using Pearson correlation analysis, r indicated Pearson correlation coefficient). MPO myeloperoxidase, MMP matrix metalloproteinase

also positively correlated with clinical score ($r = 0.88$, $P = 0.001$, $n = 10$, Fig. 3c, lower panel).

Interestingly, FMT-MRI fused imaging found in vivo MPO-Gd and MMPsense signal co-localized in both ABAH-treated and saline-treated mice (Fig. 3a). In ABAH-treated EAE group, the mean MMPsense concentration was significantly lower at 29.4 ± 4 nM ($n = 10$) vs. 41.1 ± 4 nM in the saline-treated EAE group ($n = 10$) (Fig. 3b, middle panel, $P = 0.003$). Activated total MMPSense (pmol) was similarly significantly decreased in ABAH-treated EAE mice compared to saline-treated mice (Fig. 3b, right panel, $P = 0.04$). Therefore, there was concordant reduced MMP activity in

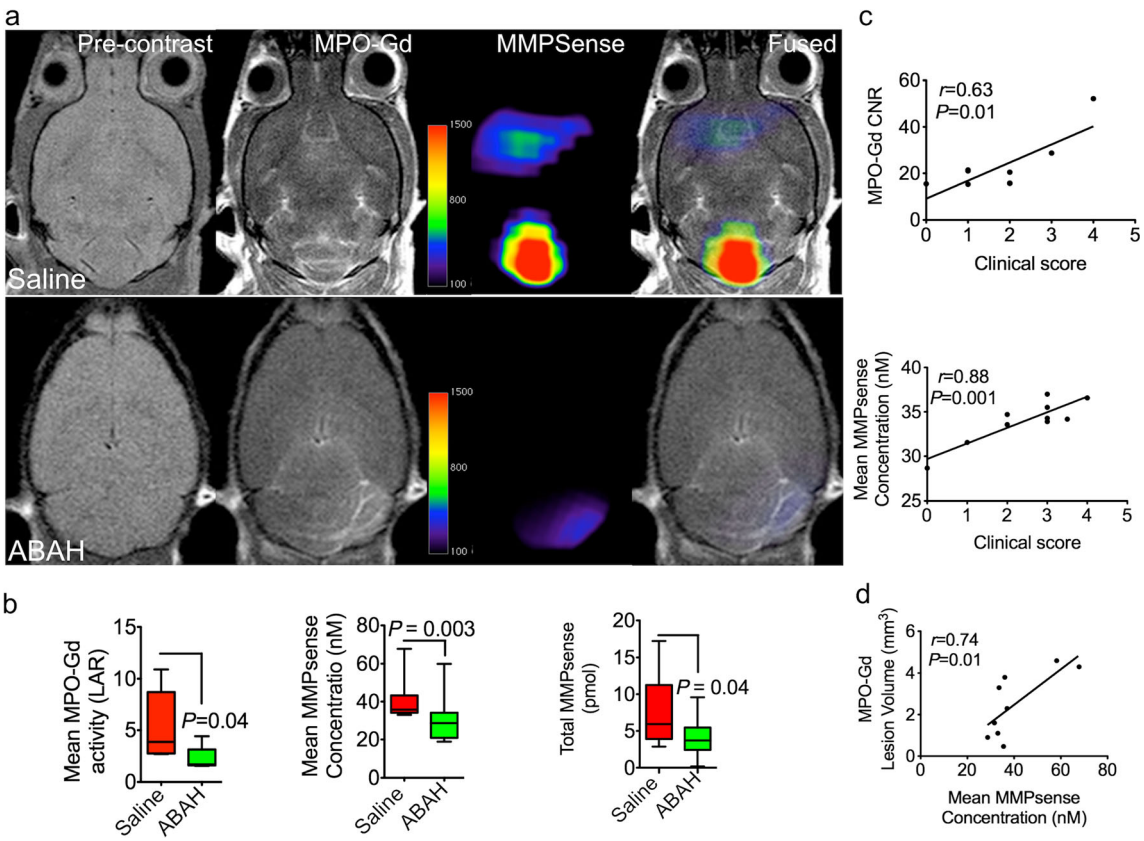

Fig. 3 In vivo mapping and regulation of MPO on MMP activity using MRI/FMT multimodal imaging. **a** Representative MRI/FMT fusion images show that in vivo MPO and MMP activity both increased in EAE mice, and both MPO and MMP activities were partially blocked with the MPO inhibitor 4-aminobenzoic acid hydrazide (ABAH). **b** MPO-Gd activation from MRI decreased with MPO inhibition, $n = 10$ per group, Mann-Whitney test, left panel). Mean fluorescence of MMPsense signal between saline-treated and ABAH-treated EAE mice ($n = 10$ per group, Mann-Whitney test, middle panel). Total activated MMPsense probe significantly decreased with MPO inhibition in EAE mice (Mann-Whitney test, right panel). **c** Contrast-to-noise ratio (CNR) from MRI images correlated with clinical score ($n = 7$) (upper panel). MMP activity from FMT images (mean MMPsense concentration) positively correlated with clinical score ($n = 10$, Pearson correlation analysis) (low panel). **d** MPO-Gd$^+$ lesion volume positively correlated with MMPsense concentration ($n = 9$, data were obtained by using Pearson correlation analysis, r indicated Pearson correlation coefficient). All data are means ± standard errors of measurement. CNR contrast noise ratio, LAR lesion activation ratio, MPO myeloperoxidase, MMP matrix metalloproteinase

brains of EAE mice after MPO inhibition. In addition, a significant positive correlation was observed between MPO-Gd$^+$ lesion volume and mean MMPsense concentration ($r = 0.74$, $P = 0.01$, $n = 9$, Fig. 3d).

MPO Inhibition Affects MMP-Positive Cells

We next assessed what effects MPO inhibition has on MMP-secreting cells. On flow cytometry, we found that with MPO inhibition, the number of cells positive for MMP activity in EAE mice (34% ± 5%) decreased in the ABAH-treated group (15% ± 3%, $P = 0.009$, $n = 5$ per group, Fig. 4a). Both the number of MMM cells and neutrophils ($(1.1 \pm 0.1) \times 10^6$ vs $(0.5 \pm 0.1) \times 10^6$, $P = 0.008$ and $(0.03 \pm 0.01) \times 10^6$ vs $(0.01 \pm 0.004) \times 10^6$, $P = 0.03$, Fig. 4b, respectively) significantly decreased with MPO inhibition ($(7.8 \pm 1.1) \times 10^5$ vs $(2.9 \pm 0.8) \times 10^5$ of inflammatory macrophage/activated microglia in saline and ABAH-treated group, $P = 0.036$; $(3 \pm 0.4) \times 10^5$ vs $(1.7 \pm 0.2) \times 10^5$ of resident microglia in saline and ABAH-treated group, $P = 0.04$, $n = 5$ per group, Fig. 4c).

Further corroborating the above results, immunohistochemistry showed that there were fewer MPO$^+$ (1371 ± 411 vs 528 ± 133, $P = 0.023$, $n = 5$ per group, Fig. 5a, b, upper panel) and MMP-9$^+$ cells (469 ± 123 vs 209 ± 38, $P = 0.019$, $n = 5$ per group, Fig. 5a, b, low panel) in EAE animals when MPO was blocked by ABAH compared to saline-treated group (Fig. 5a, quantified in 5b, $P = 0.023$ and $P = 0.019$, respectively). The majority of MPO$^+$ cells co-localized with MMP-9$^+$ cells on immunofluorescence (Fig. 5c), although MMP expression in some cells, appeared to be less compared to that of MPO. We found the number of MPO$^+$ cells highly correlated with the number of MMP$^+$ cells ($r = 0.91$, $P < 0.0001$, $n = 6$, Fig. 5d).

In Vitro Validation of MPO Regulation of Matrix Metalloproteinase

We further validated our in vivo findings on MPO regulation of MMP activity in EAE using in vitro assays. We first

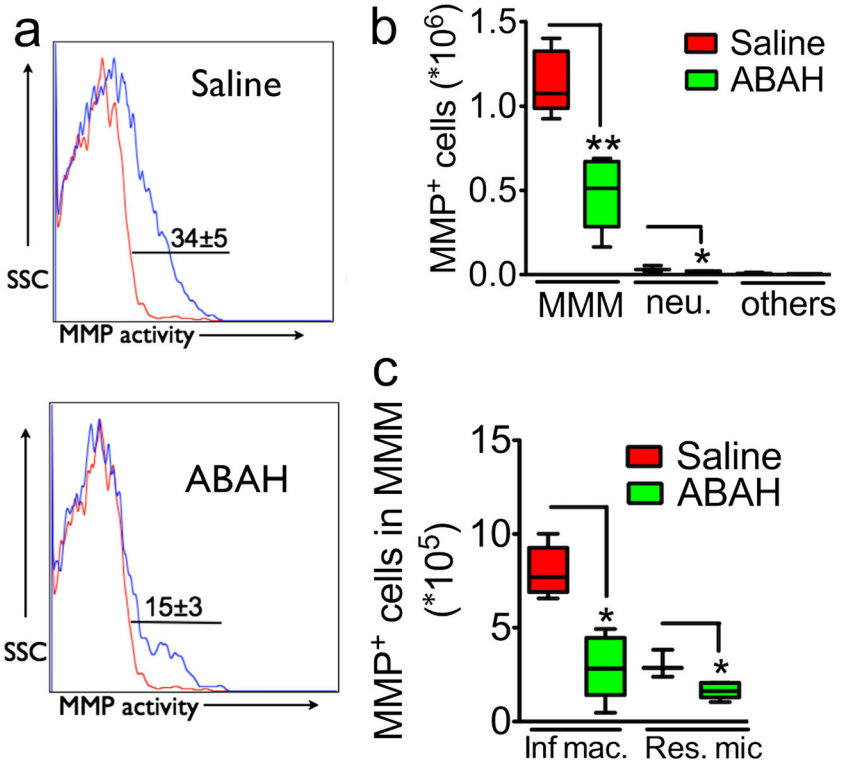

Fig. 4 The effects of 4-aminobenzoic acid hydrazide (ABAH) on MMP+ cells. **a** Cell surface markers used to subdivide cells into various subsets of leukocytes in the brain of saline-treated control and ABAH-treated EAE mice 12 days after immunization. Numbers denote percent MMP-positive cells in saline (34% ± 5%) versus ABAH group (15% ± 3%) ($P = 0.009$, $n = 5$ per group, two-tailed Student's t test) (red line: percent MMP-positive cells in sham mice; blue line: percent MMP-positive cells in EAE mice). **b** Total MMP-positive cell counts in the brain. There are significant differences between saline and ABAH group in cell number of microglia/monocytes/macrophages and neutrophils (Mann-Whitney test, $^{**}P = 0.007$ and $^{**}P = 0.04$). **c** Contribution of cell types to MMP activity in EAE based on results in **a** and **b**. MMP matrix metalloproteinase

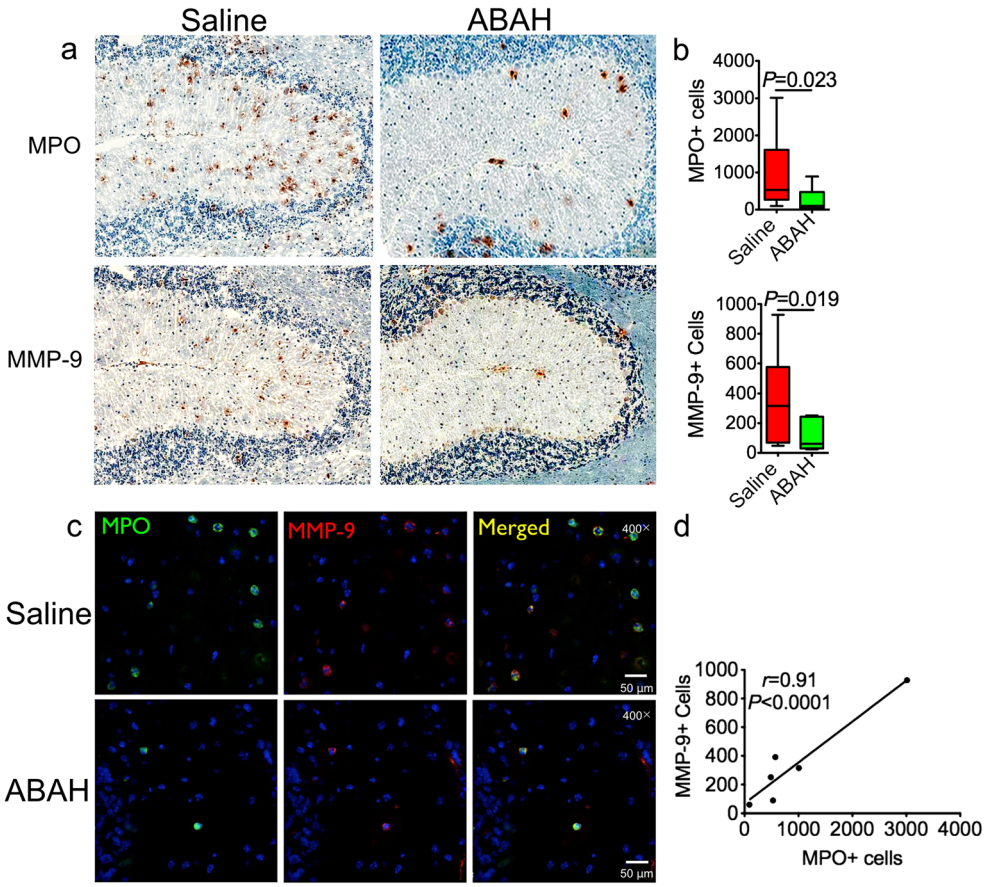

Fig. 5 MPO- and MMP-9-positive cells are reduced with MPO inhibition. **a** Photomicrographs (immunohistochemistry, scale bar = 200 μm [original magnification ×100]) from the cerebellum showed that MPO- (upper panel) and MMP-9 (low panel)-positive cells are decreased with MPO inhibition. **b** Quantification of **a** ($n = 5$ per group, Mann-Whitney test). The average total number of positive cells from the entire brain on three different sections for each mouse was used for quantification. **c** Photomicrographs (immunofluorescence staining, scale bar = 500 μm [original magnification ×400], cerebellum) showed most of MPO-positive cells co-localized with MMP-positive cells. d MPO-positive cells correlated with MMP-positive cells ($n = 6$, Pearson correlation analysis, r indicated Pearson correlation coefficient). MPO myeloperoxidase, MMP matrix metalloproteinase

verified that ABAH reduced the MPO activity in the EAE brain (saline 0.023 ± 0.002 U/mg vs. ABAH 0.018 ± 0.001 U/mg, Fig. 6a, $P = 0.018$, $n = 5$ per group). Similar to the in vivo findings, EAE animals treated with ABAH to block MPO activity showed significantly reduced MMP-9 activity compared to that in saline-treated controls (5.8 ± 0.2 μM vs 4.7 ± 0.4 μM, $P = 0.016$, $n = 5$ per group, Fig. 6b). Notably, treating naïve brain extracts with purified human MPO resulted in significant induction of MMP-9 activity compared to saline-treated control extracts (1.3 ± 0.04 μM vs 1.5 ± 0.1 μM, $P = 0.03$, $n = 5$ per group, Fig. 6c).

Discussion

In the present study, we confirmed for the first time in living animals that MPO and MMPs are directly correlated with each other in a neuroinflammatory disease model. We demonstrate that MPO positively regulates MMP activity in vivo. Moreover, myeloid cells contribute to most of the MMP activity in EAE, and changes in MPO activity affected MMP activity and MMP^+ cells in EAE in a concordant manner. MMP activity from FMT imaging colocalized with MPO-Gd MR imaging. These imaging metrics also correlated with clinical symptoms. Thus, combined MRI/FMT imaging of MPO and MMP activity can provide localization and quantification information on the inflamed lesions in the brain and may predict disease severity.

Since we found that MPO positively regulates MMPs in vivo and in vitro, this revealed that in vivo in neuroinflammatory conditions such as EAE, MPO, and its products predominately regulates MMPs by the activation pathways [12, 19] instead of the inhibition pathway [13, 20]. Interestingly, several in vitro studies had demonstrated that MPO-generated HOCl activates purified MMPs at ratios between 10 and 40 of HOCl/MMPs but causes inactivation of MMPs at > 40:1 ratios [21–23]. Our results revealed higher MMPsense signal in the saline-treated EAE mice compared to ABAH-treated mice, suggesting that > 40:1 ratio was not achieved in the EAE brain to cause MPO to inhibit MMP activity. The most likely explanation for our results would be that the HOCl/MMP ratio stayed within 10–40:1 both without and with MPO inhibition. In that scenario, MPO activity and MMP activity would be positively correlated, as we observed.

Myeloid cells are important sources of MPO, MMP, and TIMP in EAE [24]. Macrophage infiltration is required for EAE and if blocked, can prevent disease [25]. We found that inflammatory myeloid cells contribute to most of the MMP activity, which in turn correlated well with clinical scores. On immunofluorescence imaging, most of the MPO+ cells co-localized with MMP+ cells. However, a few cells were only

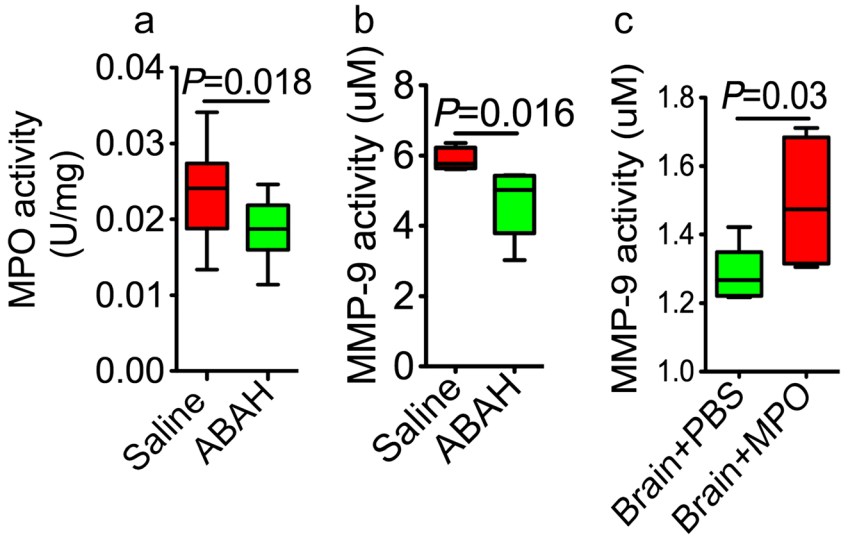

Fig. 6 In vitro validation of MPO regulation of matrix metalloproteinases. **a** MPO activity decreased with MPO inhibition ($P = 0.018$, $n = 5$ per group, Mann-Whitney test). **b** MMP-9 activity decreased with MPO inhibition in EAE ($P = 0.016$, $n = 5$ per group, Mann-Whitney test). **c** MMP-9 activity was significantly elevated with MPO (10 μg/ml) stimulation in vivo ($P = 0.03$, $n = 5$ per group, Mann-Whitney test). All data are means ± standard errors of measurement. MPO myeloperoxidase, MMP matrix metalloproteinase, ABAH 4-aminobenzoic acid hydrazide

MPO+ but did not express MMP. This indicates that only a subset of MPO+ cells express MMP. Given that prior studies found that MMP in the inflamed brain is mainly made by infiltrating myeloid cells [26], these MPO+-only cells are likely resident microglia. MMP-9 has previously been reported to be up-regulated in both mouse and rat EAE [27, 28]. When we inhibited MPO with the specific irreversible MPO inhibitor ABAH, MMP activity was also inhibited, as seen in both in vivo imaging and in vitro activity assays. Thus, MPO-rich inflammatory macrophages/microglia likely promote inflammation and tissue destruction through the activation of MMPs, which disrupt BBB and further the inflammatory cascade to exacerbate clinical outcomes. On the other hand, inhibiting MPO activity decreased MMP activity and BBB breakdown, resulting in decreased leukocyte infiltration and improved clinical outcomes. Taken together, our results add a mechanistic link between MPO, inflammation/leukocyte recruitment, and MMPs in EAE.

A limitation of our study is that while MMPsense is sensitive and specific to MMPs, it detects multiple different MMPs, including MMP-2, -3, -9, and -13. Thus, whether MPO affects only one (e.g., MMP-9) or many of these MMPs in vivo is currently unknown. Another limitation is that EAE is an artificial neuroinflammatory disease in animals and may not correspond to any human disease. However, EAE has been widely used to study neuroinflammation and MS, and treatment drugs for MS have been developed using EAE, suggesting that EAE is a relevant disease model for at least multiple sclerosis. While fluorescent imaging currently has limited depth of penetration, theoretical studies suggested that near infrared signal used by probes such as MMPsense can penetrate through large human organs [29]. Recent development has seen fluorescent imaging of atherosclerosis using a catheter-based detector system [30]. Thus, future technological advances will likely further improve its clinical utility. Furthermore, nuclear imaging agents for MMPs have also been recently developed [4].

The combined use of MPO MRI and MMP FMT imaging noninvasively informed on the relationship between MPO and MMP activity in vivo and correlated these in vivo inflammatory markers with disease severity. The results of our study attest to the sensitivities of these technologies in discriminating between different levels of inflammatory burden and suggest a role in assessing treatment efficacy. In conclusion, multimodal molecular imaging demonstrates for the first time in vivo MPO regulation of MMP activity in living animals and offers a sensitive and quantifiable approach to assess and track disease activity in experimental neuroinflammatory models relevant to neurological diseases such as MS. This approach could serve as a model to study the interactions of other biologically interesting molecules in living organisms.

Source of Funding This study was supported by the NIH (R01-NS070835 and R01-NS072167, to JWC), the National Multiple Sclerosis Society (JWC), the National Natural Science Foundation of China (81771297 and 81501116, to YZ), and Cuiying Scientific and Technological Innovation Program of Lanzhou University Second Hospital (CY2017-MS04).

References

1. Hu J, Van den Steen PE, Sang QX, Opdenakker G (2007) Matrix metalloproteinase inhibitors as therapy for inflammatory and vascular diseases. Nat Rev Drug Discov 6(6):480–498. https://doi.org/10.1038/nrd2308
2. Maier CM, Hsieh L, Yu F, Bracci P, Chan PH (2004) Matrix metalloproteinase-9 and myeloperoxidase expression: quantitative analysis by antigen immunohistochemistry in a model of transient focal cerebral ischemia. Stroke 35(5):1169–1174. https://doi.org/10.1161/01.STR.0000125861.55804.f2
3. Parks WC, Wilson CL, Lopez-Boado YS (2004) Matrix metalloproteinases as modulators of inflammation and innate immunity. Nat Rev 4(8):617–629
4. Gerwien H, Hermann S, Zhang X, Korpos E, Song J, Kopka K, Faust A, Wenning C et al (2016) Imaging matrix metalloproteinase activity in multiple sclerosis as a specific marker of leukocyte penetration of the blood-brain barrier. Sci Transl Med 8(364):364ra152. https://doi.org/10.1126/scitranslmed.aaf8020
5. Sorokin L (2010) The impact of the extracellular matrix on inflammation. Nat Rev 10(10):712–723
6. Opdenakker G, Nelissen I, Van Damme J (2003) Functional roles and therapeutic targeting of gelatinase B and chemokines in multiple sclerosis. Lancet Neurol 2(12):747–756
7. Fainardi E, Castellazzi M, Bellini T, Manfrinato MC, Baldi E, Casetta I, Paolino E, Granieri E et al (2006) Cerebrospinal fluid and serum levels and intrathecal production of active matrix metalloproteinase-9 (MMP-9) as markers of disease activity in patients with multiple sclerosis. Mult Scler 12(3):294–301
8. van der Veen BS, de Winther MP, Heeringa P (2009) Myeloperoxidase: molecular mechanisms of action and their relevance to human health and disease. Antioxid Redox Signal 11(11):2899–2937
9. Swirski FK, Weissleder R, Pittet MJ (2009) Heterogeneous in vivo behavior of monocyte subsets in atherosclerosis. Arterioscler Thromb Vasc Biol 29(10):1424–1432
10. Gray E, Thomas TL, Betmouni S, Scolding N, Love S (2008) Elevated activity and microglial expression of myeloperoxidase in demyelinated cerebral cortex in multiple sclerosis. Brain Pathology (Zurich, Switzerland) 18(1):86–95
11. Fu X, Kassim SY, Parks WC, Heinecke JW (2001) Hypochlorous acid oxygenates the cysteine switch domain of pro-matrilysin (MMP-7). A mechanism for matrix metalloproteinase activation and atherosclerotic plaque rupture by myeloperoxidase. J Biol Chem 276(44):41279–41287
12. Wang Z, Nicholls SJ, Rodriguez ER, Kummu O, Horkko S, Barnard J, Reynolds WF, Topol EJ et al (2007) Protein carbamylation links inflammation, smoking, uremia and atherogenesis. Nat Med 13(10):1176–1184
13. Fu X, Kassim SY, Parks WC, Heinecke JW (2003) Hypochlorous acid generated by myeloperoxidase modifies adjacent tryptophan and glycine residues in the catalytic domain of matrix metalloproteinase-7 (matrilysin): an oxidative mechanism for restraining proteolytic activity during inflammation. J Biol Chem 278(31):28403–28409
14. McCann CM, Waterman P, Figueiredo JL, Aikawa E, Weissleder R, Chen JW (2009) Combined magnetic resonance and fluorescence imaging of the living mouse brain reveals glioma response to chemotherapy. Neuroimage 45(2):360–369. https://doi.org/10.1016/j.neuroimage.2008.12.022
15. Forghani R, Wojtkiewicz GR, Zhang Y, Seeburg D, Bautz BR, Pulli B, Milewski AR, Atkinson WL et al (2012) Demyelinating diseases: myeloperoxidase as an imaging biomarker and therapeutic target. Radiology 263(2):451–460. https://doi.org/10.1148/radiol.12111593
16. Chen JW, Querol Sans M, Bogdanov A Jr, Weissleder R (2006) Imaging of myeloperoxidase in mice by using novel amplifiable paramagnetic substrates. Radiology 240(2):473–481
17. Rodriguez E, Nilges M, Weissleder R, Chen JW (2010) Activatable magnetic resonance imaging agents for myeloperoxidase sensing: mechanism of activation, stability, and toxicity. J Am Chem Soc 132(1):168–177. https://doi.org/10.1021/ja905274f
18. Breckwoldt MO, Chen JW, Stangenberg L, Aikawa E, Rodriguez E, Qiu S, Moskowitz MA, Weissleder R (2008) Tracking the inflammatory response in stroke in vivo by sensing the enzyme myeloperoxidase. Proc Natl Acad Sci U S A 105(47):18584–18589. https://doi.org/10.1073/pnas.0803945105
19. Teng N, Maghzal GJ, Talib J, Rashid I, Lau AK, Stocker R (2017) The roles of myeloperoxidase in coronary artery disease and its potential implication in plaque rupture. Redox Rep 22(2):51–73. https://doi.org/10.1080/13510002.2016.1256119
20. Vissers MC, Winterbourn CC (1987) Myeloperoxidase-dependent oxidative inactivation of neutrophil neutral proteinases and microbicidal enzymes. Biochem J 245(1):277–280
21. Mainnemare A, Megarbane B, Soueidan A, Daniel A, Chapple IL (2004) Hypochlorous acid and taurine-N-monochloramine in periodontal diseases. J Dent Res 83(11):823–831. https://doi.org/10.1177/154405910408301101
22. Michaelis J, Vissers MC, Winterbourn CC (1992) Different effects of hypochlorous acid on human neutrophil metalloproteinases: activation of collagenase and inactivation of collagenase and gelatinase. Arch Biochem Biophys 292(2):555–562
23. Davies JM, Horwitz DA, Davies KJ (1994) Inhibition of collagenase activity by N-chlorotaurine, a product of activated neutrophils. Arthritis Rheum 37(3):424–427
24. Toft-Hansen H, Nuttall RK, Edwards DR, Owens T (2004) Key metalloproteinases are expressed by specific cell types in experimental autoimmune encephalomyelitis. J Immunol 173(8):5209–5218
25. Martiney JA, Rajan AJ, Charles PC, Cerami A, Ulrich PC, Macphail S, Tracey KJ, Brosnan CF (1998) Prevention and treatment of experimental autoimmune encephalomyelitis by CNI-1493, a macrophage-deactivating agent. J Immunol 160(11):5588–5595
26. Wang G, Guo Q, Hossain M, Fazio V, Zeynalov E, Janigro D, Mayberg MR, Namura S (2009) Bone marrow-derived cells are the major source of MMP-9 contributing to blood-brain barrier dysfunction and infarct formation after ischemic stroke in mice. Brain Res 1294:183–192. https://doi.org/10.1016/j.brainres.2009.07.070
27. Pagenstecher A, Stalder AK, Kincaid CL, Shapiro SD, Campbell IL (1998) Differential expression of matrix metalloproteinase and tissue inhibitor of matrix metalloproteinase genes in the mouse central nervous system in normal and inflammatory states. Am J Pathol 152(3):729–741
28. Clements JM, Cossins JA, Wells GM, Corkill DJ, Helfrich K, Wood LM, Pigott R, Stabler G et al (1997) Matrix metalloproteinase expression during experimental autoimmune encephalomyelitis and effects of a combined matrix metalloproteinase and tumour necrosis factor-alpha inhibitor. J Neuroimmunol 74(1–2):85–94
29. Ntziachristos V, Ripoll J, Weissleder R (2002) Would near-infrared fluorescence signals propagate through large human organs for clinical studies? Opt Lett 27(5):333–335
30. Yoo H, Kim JW, Shishkov M, Namati E, Morse T, Shubochkin R, McCarthy JR, Ntziachristos V et al (2011) Intra-arterial catheter for simultaneous microstructural and molecular imaging in vivo. Nat Med 17(12):1680–1684. https://doi.org/10.1038/nm.2555